



Adjoint-based shape sensitivity of multi-row turbomachinery

Simão S. Rodrigues¹ · André C. Marta¹

Received: 6 March 2019 / Revised: 5 July 2019 / Accepted: 7 August 2019
© Springer-Verlag GmbH Germany, part of Springer Nature 2019

Abstract

The performance sensitivity of a low-pressure turbine stator-rotor stage of a commercial jet engine to its blades and hub shapes is analyzed. The derivatives of various metrics, such as isentropic efficiency, total pressure ratio, total pressure loss, and loss coefficient are computed using an adjoint solver capable of handling multi-row analyses. The importance of considering the coupled stator-rotor stage is highlighted from the computed sensitivities, which reveal that performing individual stator or rotor row component optimization may lead to an unexpected performance loss of the whole stage. The obtained coupled sensitivities are then used in an endwall contouring application, consisting of two Hicks-Henne bumps applied on the hub surface of the rotor to maximize stage efficiency, at locations selected where the impact is found to be the highest from the adjoint-based sensitivity analysis. The performance gain obtained with the bumps is correlated to the changes in the flow field, in particular with the effect on secondary flows.

Keywords Multistage coupling · Sensitivity analysis · Aerodynamic shape optimization · Endwall contouring · Gas turbine · Jet engine

1 Introduction

As computational power has been rapidly increasing and with the advances in numerical methods, the use of high-fidelity computational fluid dynamics (CFD) tools in the design of turbomachinery has also increased, becoming more and more common, particularly in numerical optimization environments.

The choice of the optimization algorithm often dictates the selected approach for the analysis of the flow. Optimization problems in turbomachinery typically consist in a large number of design variables and, as such, the computational cost inherited from the high-dimensional design space must be taken into account. Heuristic gradient-free methods, such as genetic algorithms or differential evolution, can be an important tool for early design stages (Chirkov et al. 2018; Joly et al. 2014), when a new

rough design is being developed, as they are able to find minima without being stuck in local minima close to the initial conditions. In such cases, the use of surrogate models is often employed as it greatly reduces the optimization cost in terms of CPU time (Pierret et al. 2007; Yu et al. 2011; Benamara et al. 2017). In later stages of the design process, gradient-based algorithms offer a big advantage since they are much more computationally efficient, both in terms of reduced number of function evaluations and convergence of the optimal solution. However, as their name implies, they imply computing the gradients of the functions of interest with respect to the design variables. Traditional methods such as finite-difference approximations present a computational cost proportional to the number of design variables. For large number of the later, an efficient method to compute these gradients is essential to maintain acceptable computational requirements.

The adjoint method applies control theory to the flow governing equations to obtain a linear system of equations—the adjoint system of equations—whose solution can be used to compute the total derivatives of functions of interest, often called sensitivities, with a computational cost that is nearly independent of the number of design variables. It was first introduced by Pironneau (1974) in CFD and further extended by Jameson (1988) to optimization of airfoil profiles and wings and full aircraft geometry (Jameson et al. 1998, 2004). Its efficiency in

Responsible Editor: Jianbin Du

✉ Simão S. Rodrigues
simao.rodrigues@tecnico.ulisboa.pt

André C. Marta
andre.marta@tecnico.ulisboa.pt

¹ IDMEC, Instituto Superior Técnico, Universidade de Lisboa, Av. Rovisco Pais 1, 1049 Lisboa, Portugal

computing sensitivities in problems with high number of design variables has made it the choice in a wide range of subjects. Particularly in turbomachinery, many authors have used adjoint-based gradients in numerical optimization frameworks (Walther and Nadarajah 2015; Backhaus et al. 2017).

Being very complex mechanisms, many approaches can be taken to increase the performance of turbomachinery such as the control of the inlet/exit conditions (Marta and Shankaran 2014), the modification of the shape of the blades (Duan et al. 2018) and/or endwall regions (Poehler et al. 2015), or the use of higher performance materials (Min et al. 2011).

While the blades are responsible for the primary flow structures, and their shape is carefully tuned to obtain the desired pressure ratios (Mueller and Verstraete 2017), the efficiency of a turbomachine is often dictated by the so-called secondary flows. The flow inside turbomachine components is highly three-dimensional (3D) and unsteady, particularly in high-pressure compressors with high blade loading and small aspect ratio blades (Beselt et al. 2014). However, even in low-pressure turbine components (Schneider et al. 2013), the endwall (hub and casing) regions can be affected by 3D phenomena such as the tip clearance vortex or the horseshoe vortex, that are responsible for the loss of performance of the turbine or compressor. As such, by properly controlling the flow in these critical regions, the losses can be minimized.

One way of controlling the secondary flows is by means of modifying the geometry of the the hub and casing surfaces, also known as endwall contouring, which can bring significant reduction of the secondary losses. Many works addressing this topic can be found in the literature, such those of Sauer et al. (2001) that reduced secondary losses due to horseshoe vortex by imposing an endwall bulb near the leading edge, Corral and Gisbert (2008) that optimized the endwall profile of a low-pressure turbine (LPT) row using the discrete adjoint-based gradients to reduce the secondary kinetic energy, Luo et al. (2015) that applied continuous adjoint-based sensitivities to the optimization of a single turbine blade row through endwall contouring, or even Reutter et al. (2017) that used NURBS to parameterize the hub of a low-pressure turbine in a multi-point optimization environment.

It should be noted that most axial turbomachinery are composed of multiple stages, each composed of a stator and a rotor rows, in order to compress and expand the flow at even higher pressure ratios. However, the typical blade shape optimization or endwall contouring, such as those described previously, considers only a single row, keeping the inlet and boundary conditions frozen. From first principles of fluid mechanics, in subsonic flows, the flow perturbations propagate not only downstream but also

upstream. This implies that any design change of a row part will have an effect on both neighboring rows. For instance, optimizing a turbine rotor row for maximum efficiency can theoretically have a detrimental impact not only in the downstream but also in the upstream stator rows, leading eventually to an overall worse stage efficiency. Consequently, it is paramount to consider the row coupling effects when performing multi-row turbomachinery design optimization. This is the focus that we try to address in this work.

In this paper, we present the results of the application of an adjoint solver capable of handling multi-row domains (Rodrigues and Marta 2018) to conduct the sensitivity analysis of the exit mass flow, the isentropic efficiency, and total pressure ratio of a low-pressure turbine stator-rotor stage to blade and hub geometry changes. We analyze the adjoint-based sensitivities to obtain insight on which direction should the geometry of the blades and hub be modified to improve the performance of the stage. Furthermore, we use the sensitivity to hub shape of the rotor to select the locations where two bumps are imposed on the baseline geometry to try to mitigate some possible secondary flows that exist on the turbine and thus improve the stage efficiency. A grid-perturbation sensitivity is chained with the adjoint-based sensitivities to obtain numerical gradients of the parameters defining the height of the bumps, and a line search procedure is performed manually to find suitable bump perturbation that are close to the possible maximum along the direction defined by the gradient. Following this, we analyze and discuss the flow obtained from the modified geometry, highlighting the features of the flow that were changed due to the shape perturbations and the coupling effects among blade rows.

2 Background

The typical problem in which shape sensitivity information is applied in turbomachinery is included in either the design phase of a new turbomachine blade, or the modification of a legacy geometry to improve performance. Both problems can be represented by an optimization problem, defined mathematically as

$$\begin{aligned} & \text{minimize } \mathcal{I}(\boldsymbol{\alpha}, \mathbf{q}(\boldsymbol{\alpha})) \\ & \text{w.r.t. } \boldsymbol{\alpha}, \\ & \text{subject to } \mathcal{C}(\boldsymbol{\alpha}, \mathbf{q}(\boldsymbol{\alpha})) \leq 0 \\ & \text{and } \mathcal{R}(\boldsymbol{\alpha}, \mathbf{q}(\boldsymbol{\alpha})) = 0, \end{aligned} \quad (1)$$

where \mathcal{I} is the set of objective functions (or performance metrics) to be minimized/maximized, $\boldsymbol{\alpha}$ is the set of design variables, \mathbf{q} is the solution obtained from solving the flow-governing equations represented by \mathcal{R} , and \mathcal{S} represents

the possible set of constrains. The objective functions and constraints might depend directly on the set of design variables, and also via the their dependency on the solution \mathbf{q} , if such exists.

2.1 Flow-governing equations

The present work uses the Reynolds-averaged Navier-Stokes (RANS) equations to model the flow. In conservative form, the Navier-Stokes equations can be written as

$$\frac{\partial \rho}{\partial t} + \frac{\partial}{\partial x_j} (\rho u_j) = 0, \quad (2a)$$

$$\frac{\partial}{\partial t} (\rho u_i) + \frac{\partial}{\partial x_j} (\rho u_i u_j + p \delta_{ij} - \tau_{ji}) = 0 \quad (2b)$$

and

$$\frac{\partial}{\partial t} (\rho E) + \frac{\partial}{\partial x_j} (\rho E u_j + p u_j - u_i \tau_{ij} + q_j) = 0, \quad (2c)$$

where ρ is the density, u_i is the mean velocity in i direction, E the total energy, p is the pressure, τ_{ij} is the viscous stress, and q_j is the heat flux. Reynolds stresses are modeled with Wilcox's two equation $k - \omega$ model (Wilcox 2008),

$$\begin{aligned} \frac{\partial}{\partial t} (\rho k) + \frac{\partial}{\partial x_j} (\rho k u_j) &= \tau_{ij} \frac{\partial u_i}{\partial x_j} - \beta_k \rho k \omega \\ &+ \frac{\partial}{\partial x_j} \left[\left(\mu + \sigma_k \frac{\rho k}{\omega} \right) \frac{\partial k}{\partial x_j} \right] \end{aligned} \quad (3a)$$

and

$$\begin{aligned} \frac{\partial}{\partial t} (\rho \omega) + \frac{\partial}{\partial x_j} (\rho \omega u_j) &= \frac{\gamma \omega}{k} \tau_{ij} \frac{\partial u_i}{\partial x_j} - \beta_\omega \rho \omega^2 \\ &+ \frac{\partial}{\partial x_j} \left[\left(\mu + \sigma_\omega \frac{\rho k}{\omega} \right) \frac{\partial \omega}{\partial x_j} \right], \end{aligned} \quad (3b)$$

where ω is the specific dissipation rate and k is the turbulence kinetic energy, and the constants are $\gamma = 5/9$, $\beta_k = 9/100$, $\beta_\omega = 3/40$, $\sigma_k = 1/2$, and $\sigma_\omega = 1/2$. The effective viscosity is computed as a sum of a laminar and turbulent term, $\mu = \mu_l + \mu_t$, with μ_t computed as $\mu_t = \rho k / \omega$ and μ_l obtained from the Sutherland's law. To account for the near-wall viscous effects, a wall function method is used to model the boundary layer, namely the standard model without pressure gradients (Launder and Spalding 1972). Wall integration is also available in the solver but it was not chosen as it would dramatically increase the computational cost due to the required finer meshes.

In their discretized form, the RANS equations can be written as

$$\frac{dq_{ijk}}{dt} + \mathbf{R}_{ijk}(\mathbf{q}) = 0, \quad (4)$$

where and the triad ijk represents the three computational directions. As this work deals with the steady RANS

equations, the unsteady term is dropped through the rest of this paper.

2.2 Adjoint equations

The adjoint system of equations (Giles and Pierce 2000) can be defined as

$$\left[\frac{\partial \mathbf{R}}{\partial \mathbf{q}} \right]^T \boldsymbol{\psi} = \left[\frac{\partial \mathcal{I}}{\partial \mathbf{q}} \right]^T, \quad (5)$$

from which the solution $\boldsymbol{\psi}$ can be used to compute the derivative of the function of interest \mathcal{I} to a set of arbitrary design variables $\boldsymbol{\alpha}$ as

$$\frac{d\mathcal{I}}{d\boldsymbol{\alpha}} = \frac{\partial \mathcal{I}}{\partial \boldsymbol{\alpha}} - \boldsymbol{\psi}^T \frac{\partial \mathbf{R}}{\partial \boldsymbol{\alpha}}. \quad (6)$$

Since there is no dependency on \mathbf{q} in (6), the adjoint solution $\boldsymbol{\psi}$ can be used to compute derivatives of a specific function of interest to various sets of design variables without any additional solution of the adjoint system of equations, or flow governing equations.

The treatment of the turbulence equation in the adjoint formulation can either consider full or frozen turbulence (Marta and Shankaran 2013). In this work, the complete RANS equations were handled in the adjoint system, resulting in seven adjoint state variables.

2.3 Adjoint-based shape sensitivity

Equation (6) is typically used to produce the sensitivity of performance metrics \mathcal{I} to the computational grid, assuming $\boldsymbol{\alpha} = \mathbf{X} = [x, y, z]^T$, as

$$\frac{d\mathcal{I}}{d\mathbf{X}} = \frac{\partial \mathcal{I}}{\partial \mathbf{X}} - \boldsymbol{\psi}^T \frac{\partial \mathbf{R}}{\partial \mathbf{X}}. \quad (7)$$

While being the foundation for obtaining higher-end sensitivities of geometry parameters, the sensitivity of the performance metric to mesh grid $d\mathcal{I}/d\mathbf{X}$ does not provide information that can be easily analyzed as is. The designer, as well as the numerical optimizer, would be interested in the sensitivity to certain parameterization parameters which would be more easily related with the geometric features of the blade and/or allow for smoother modifications to the geometry. These can be (i) engineering specific parameters (such as curvature, stiffness or sweep), (ii) parameters that define the shape of the blade directly (such as NURBS (Mykhaskiv et al. 2018) or other CAD parameters (Agarwal et al. 2018)), and (iii) deformation techniques (such as free form deformation (Lamousin and Wagenspack 1994) or Hicks-Henne bump functions (Hicks and Henne 1978)).

To obtain the sensitivity of the performance metrics to the specific shape parameterization, the sensitivity to the grid is

multiplied by the sensitivity of the computational grid itself to the design parameters $dX/d\alpha$ following the chain rule as

$$\frac{d\mathcal{I}}{d\alpha} = \left(\frac{\partial \mathcal{I}}{\partial X} - \psi^T \frac{\partial \mathcal{R}}{\partial X} \right) \frac{dX}{d\alpha}. \quad (8)$$

For the case of parameters that define the geometry directly, particularly if black box mesh generators are used, this term can be obtained with finite-difference approximations. Given that in an automated optimization framework, the sensitivity analysis has to be performed at least once in every iteration of the gradient-based optimizer, and the use of mesh deformation techniques (Luke et al. 2012; Ding et al. 2014) might prove beneficial in terms of computational cost, in particular if the mesh regeneration is found to be computationally expensive. In that case, the sensitivity of the mesh grid nodes to the design parameters can be obtained through the chain rule as

$$\frac{dX}{d\alpha} = \frac{dX_v}{dX_s} \frac{dX_s}{d\alpha}, \quad (9)$$

where X_v represents the interior nodes of the computational mesh and X_s , the boundary (surface) nodes. The first term is obtained from the propagation of the imposed deformations from the surface to the interior of the domain, while the latter term depends on the selected deformation/parameterization approach.

In the current study, the computation of $dX/d\alpha$ follows the mesh perturbation technique, where the perturbations on the surface are first computed from a set of design parameters $\Delta X_s = f(X_s, \alpha)$ and then the perturbation propagated into the volume grid $X_v^* = f(\Delta X_s)$. The sensitivity to the design variables is then computed from the original and modified grid using first-order finite differences as

$$\frac{dX}{d\alpha} = \frac{X_v - X_v^*}{h}. \quad (10)$$

3 Description of test case

A stator-rotor stage of a low-pressure axial turbine of a commercial jet engine is used as an illustrative test case in this work. A description of the computational domain, boundary conditions, and functions of interest are presented next.

3.1 Computational domain

The multi-row computational domain consists of two individual computational domains, representing a single blade per row due to periodicity, each discretized with an O-H grid. The stator and rotor grids are divided into 15 and 14 blocks, respectively, as represented in Fig. 1, totaling 90,750

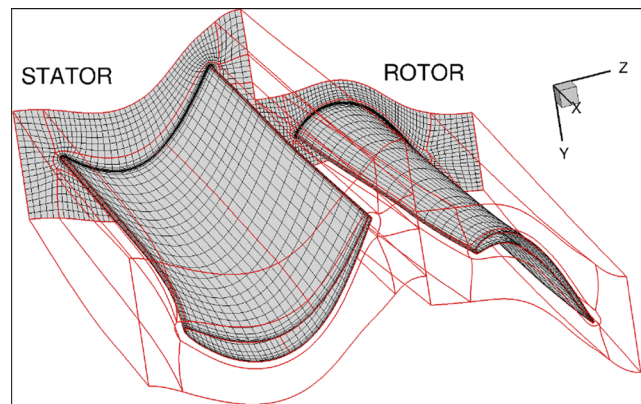


Fig. 1 Computational mesh and multi-block domain

cells. The flow is in the positive axial z -direction, being only the stator and rotor blades and the hub surfaces represented in the figure.

3.2 Boundary conditions

The stage inlet boundary conditions prescribed are absolute tangential velocity and pressure extrapolated from the interior. The stage exit static pressure is held fixed (Marta and Shankaran 2014). All solid walls are considered impermeable with no-slip condition. The remaining faces are either block-to-block interfaces or periodic.

Between the two stator-rotor domains, the boundary conditions are updated with the mixing-plane algorithm described by Holmes (2008), where the flux differences are used as a control signal to adjust the auxiliary flow variables at each side of the interface until multi-row convergence is achieved and the radial profiles at the interface between adjacent blades is very similar.

Figure 2 presents a schematic of the boundaries of the computational domain, namely, the inlet (purple), mixing-plane (green), exit (yellow), stator and rotor blade (gray), and hub surfaces (gray). The casing surface was omitted to allow for a better visualization of the various boundaries.

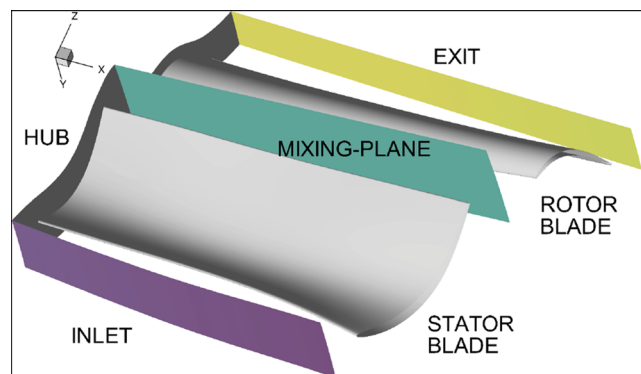


Fig. 2 Schematic of domain boundaries

3.3 Performance metrics

The sensitivity analyses of the turbomachine performance include metrics of the stator, rotor, and stage, so that coupling effects can be properly studied. In total, seven performance metrics \mathcal{I} are assessed, namely the stator loss coefficient η_{stator} , the stator total pressure loss π_{stator} , the rotor isentropic efficiency η_{rotor} , the rotor total pressure ratio π_{rotor} , the stage isentropic efficiency η_{stage} , the stage total pressure ratio π_{stage} , and the stage exit mass flow \dot{m} .

The stator loss coefficient is defined as

$$\eta_{\text{stator}} = \frac{p_{Ta}^{\text{inlet},1} - p_{Ta}^{\text{exit},1}}{p_{Ta}^{\text{inlet},1} - p_s^{\text{inlet},1}} \times 100, \quad (11)$$

where the subscripts s and Ta refer to static and total absolute quantities, respectively. The numbering in the superscripts refers to the stator (1) and rotor (2) blade passages. The stator total pressure loss is evaluated as

$$\pi_{\text{stator}} = \frac{p_{Ta}^{\text{inlet},1} - p_{Ta}^{\text{exit},1}}{p_{Ta}^{\text{inlet},1}} \times 100. \quad (12)$$

The rotor isentropic efficiency is defined as

$$\eta_{\text{rotor}} = \frac{\left(T_{Ta}^{\text{exit},2}/T_{Ta}^{\text{inlet},2}\right) - 1}{\left(p_{Ta}^{\text{exit},2}/p_{Ta}^{\text{inlet},2}\right)^{(\gamma-1)/\gamma} - 1} \quad (13)$$

and its total pressure ratio is evaluated using enthalpy averaged total pressures,

$$\pi_{\text{rotor}} = \frac{p_{Ta}^{\text{exit},2}}{p_{Ta}^{\text{inlet},2}}. \quad (14)$$

Similarly to the rotor metrics, the stage isentropic efficiency is defined by

$$\eta_{\text{stage}} = \frac{\left(T_{Ta}^{\text{exit},2}/T_{Ta}^{\text{inlet},1}\right) - 1}{\left(p_{Ta}^{\text{exit},2}/p_{Ta}^{\text{inlet},1}\right)^{(\gamma-1)/\gamma} - 1}, \quad (15)$$

and the stage total pressure ratio is given as

$$\pi_{\text{stage}} = \frac{p_{Ta}^{\text{exit},2}}{p_{Ta}^{\text{inlet},1}}, \quad (16)$$

again with the total pressure being enthalpy averaged.

The mass flow is computed at the exit of the last (rotor) blade passage.

It should be noted that, given our test case consists of a turbine stage, the design goal consists of achieving the maximum flow expansion at the highest efficiency, thus reducing the losses. The desired evolution of the performance metrics (11) to (16) is summarized in Table 1.

Table 1 Desired evolution of the performance metrics

| | Stator | Rotor | Stage |
|--------|-----------------------|-------------------------|-------------------------|
| η | Reduce (\searrow) | Increase (\nearrow) | Increase (\nearrow) |
| π | Reduce (\searrow) | Reduce (\searrow) | Reduce (\searrow) |

4 Direct and adjoint solutions

The flow-governing equations given by (4) were run to steady state with a 4th-order Runge-Kutta scheme down to a relative averaged residual of the continuity equation of 10^{-9} or less, as shown in Fig. 3. All computations were performed in double precision.

The normalized pressure field on the stator blade, rotor blade, and hub surfaces is presented in Fig. 4, viewed from two directions for the blades to show both their pressure side (PS) and suction side (SS).

The flow solution provides valuable information to the experienced designer, in particular highlighting adverse viscous or compressibility effects, such as secondary flows and shock waves, respectively. Nevertheless, in the occurrence of such undesired effects, it might not be clear what design change must be pursued to mitigate them. This is where the use of the adjoint-based sensitivity analysis tool comes handy.

With the converged flow solution, the adjoint systems of equations, given by (5), are solved for each performance metric \mathcal{I} , with a computational cost similar to solving one direct solution. The solver uses the built-in Krylov subspace method of the Portable, Extensible Toolkit for Scientific Computation (PETSc) (Balay et al. 2014), more specifically, the Generalized Minimum Residual Method (GMRES) with the incomplete factorization preconditioner with one level fill, ILU(1). The restart of the GMRES procedure was set to 75 iterations and the solution was converged down to a residual of 10^{-9} . The residual history of the GMRES algorithm is presented in Fig. 5 for some of the metrics, where effect of the restart can also be noticed.

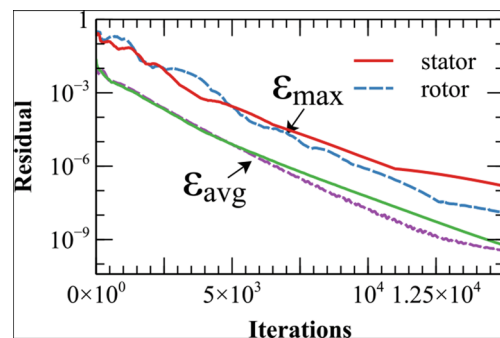


Fig. 3 Residual iteration history of flow solution

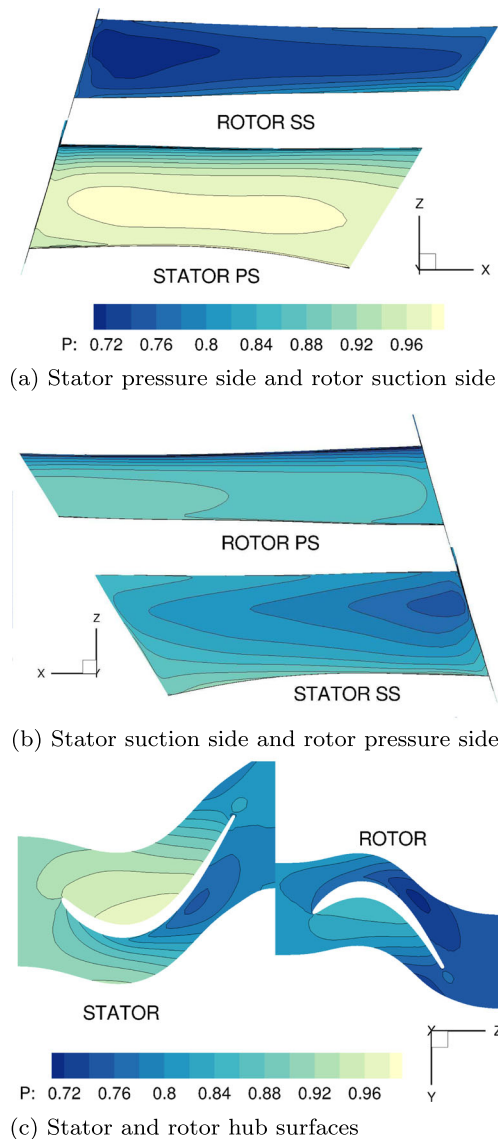


Fig. 4 Pressure field of turbine stage (normalized)

The normalized adjoint solution corresponding to the continuity equation is shown in Fig. 6, for the same geometry views as before, considering the stage isentropic efficiency as metric, $\mathcal{I} = \eta_{\text{stage}}$.

Even though it is possible to infer from the adjoint solution about the sensitivity of the turbomachine, that is not a straightforward process (Marta et al. 2013). Therefore, based on the adjoint solution, the proper performance metric sensitivities to blade shape and endwall contour are computed using (7) or (8) and (10). These sensitivities are presented in the next sections.

The adjoint-based sensitivities hereafter presented have been thoroughly verified against finite differences. This verification can be found in previous works by the

authors (Marta and Shankaran 2013; Rodrigues and Marta 2018).

5 Performance sensitivity to blade shape

The adjoint-based sensitivities of the different efficiency and pressure ratio metrics to the shape of the blades are presented in Figs. 7, 8, 9, and 10, respectively. The contour plot in these figures is the magnitude of the gradient vector projected onto the blade surface outer normal as

$$\begin{aligned} \frac{d\mathcal{I}}{d\mathbf{n}} &= \frac{d\mathcal{I}}{dx} \frac{dx}{dn} + \frac{d\mathcal{I}}{dy} \frac{dy}{dn} + \frac{d\mathcal{I}}{dz} \frac{dz}{dn} \\ &= \frac{d\mathcal{I}}{dx} n_x + \frac{d\mathcal{I}}{dy} n_y + \frac{d\mathcal{I}}{dz} n_z, \end{aligned} \quad (17)$$

where the surface outer normal unit vector is given by $\mathbf{n} = (n_x, n_y, n_z)$. In these sensitivity contour plots, and the ones following in the document, a solid line is used to identify the border between negative and positive derivatives. To better illustrate the sensitivities on the blade surfaces, Figs. 7 and 9 show the sensitivities on the stator pressure side and rotor suction side, whereas Figs. 8 and 10 present them on the stator suction side and rotor pressure side. Each of these figures contains three subfigures corresponding to the metric evaluated at the stator, rotor, and stage level.

Observing Figs. 7c–8c, and 9c–10c, it is clear that the stage efficiency is much more sensitive to the shape of the blades than the stage pressure ratio, with derivatives to blade shape in normal direction almost an order of magnitude higher for the former metric.

At the stator blade pressure side, in Figs. 7c and 9c, the derivatives of the two metrics are generally qualitatively similar, with both metrics exhibiting derivatives of stage efficiency and pressure ratio with the same sign at coincident locations, except at the stator tip mid chord. Recalling Table 1, the design goal of increasing both the stage efficiency and decreasing the stage total pressure

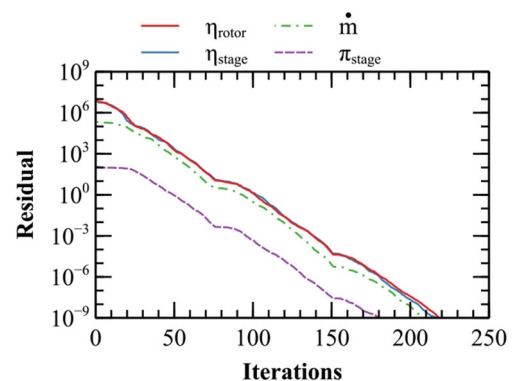


Fig. 5 Residual iteration history of adjoint solutions for different metrics

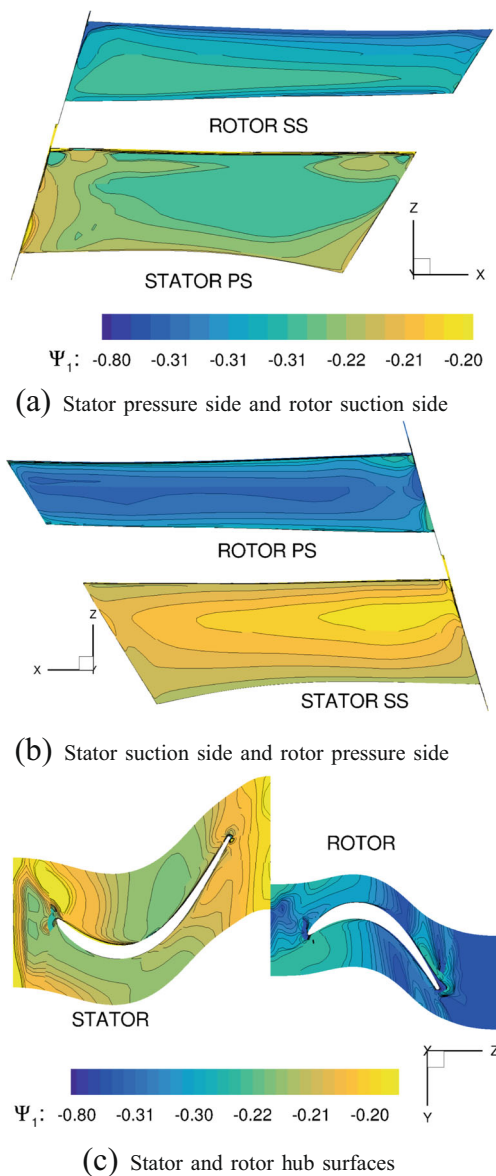


Fig. 6 Continuity adjoint field of turbine stage for $\mathcal{I} = \eta_{stage}$ (normalized)

ratio is not possible in this case as it would require derivatives with opposite signs. This observation highlights the common occurrence of competing metrics, when progressing in a certain direction of the design space (e.g., displacing the stator blade pressure side surface in one direction) would increase the stage efficiency (desired), while at the same time would also increase the stage total pressure ratio (undesired). This makes it necessary to either perform trade-off studies or to solve the optimization problem (1) considering one of the metrics as the objective \mathcal{I} and the other as a constraint \mathcal{C} , so that one is not improved at the cost of worsening the other. However, an improvement of the stage performance is possible by changing the stator blade suction side since, referring to Figs. 8c and 10c, the

sensitivity information shows that a shape displacement in the outer normal direction at the aft portion of the blade suction side leads to an increase of the stage efficiency and to a decrease of the stage total pressure ratio.

Looking at Figs. 9 and 10, the benefit of selecting a performance metric that encompasses the whole stage is evidenced by the difference in the sensitivity of the stage total pressure ratio and that of the stator total pressure loss or rotor total pressure ratio to the shape of the blades. From Fig. 9a, if the designer was to focus solely on the stator performance, then a reduction of the stator total pressure loss would be obtained by displacing the stator blade

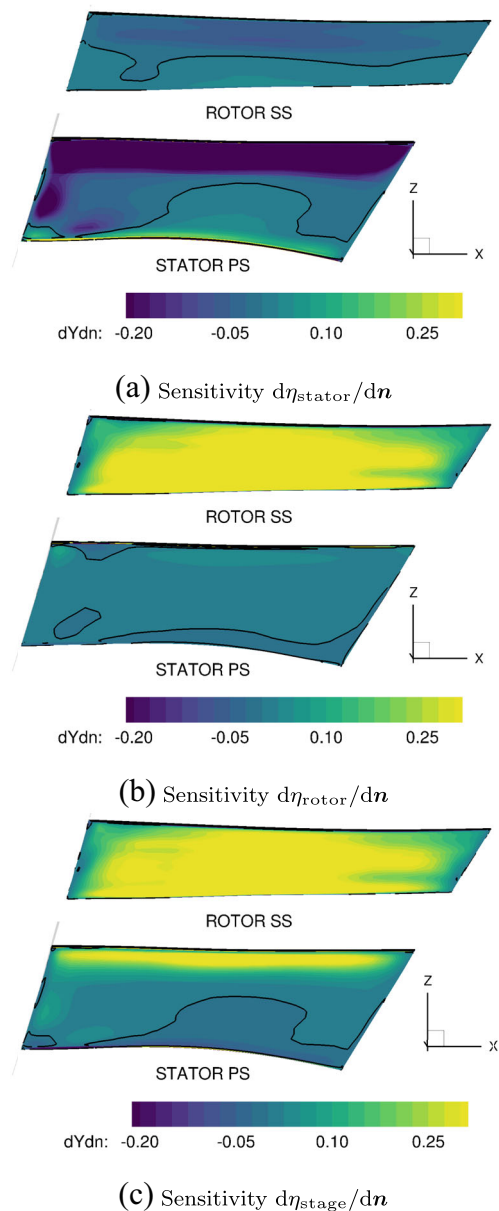


Fig. 7 Sensitivity of efficiency metrics to blade shape in normal direction—stator pressure side and rotor suction side view

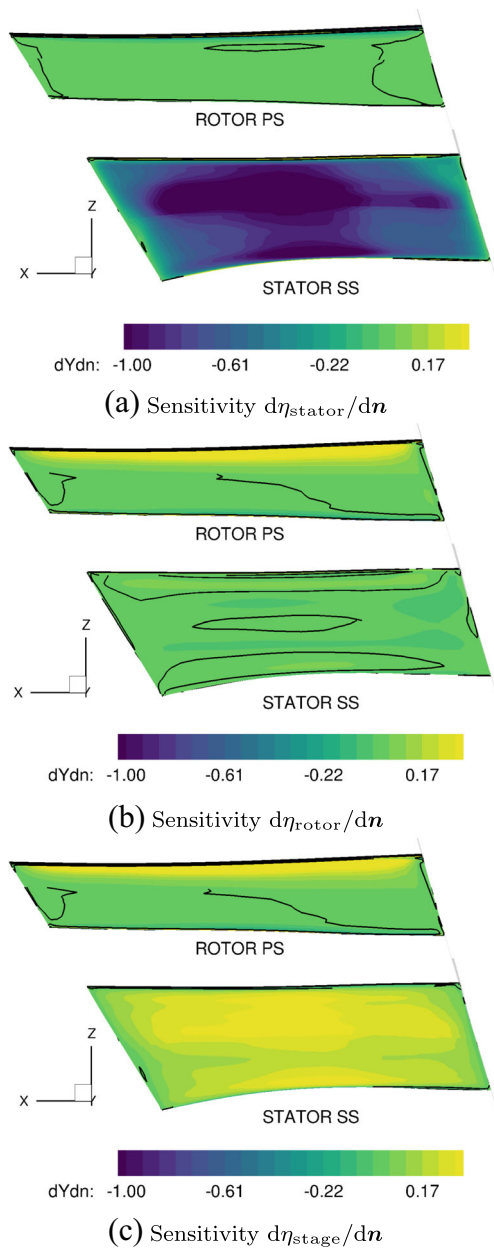


Fig. 8 Sensitivity of efficiency metrics to blade shape in normal direction—stator suction side and rotor pressure side view

pressure side outwards in the region of negative derivatives and inwards in the region of positive derivatives. However, such blade shape change would lead to an unexpected worsening of the overall stage total pressure ratio because, as seen in Fig. 9c, the sensitivity of stage pressure ratio to the stator blade shape on the pressure side is opposite in sign up to roughly 80% span. A similar unexpected behavior is also found by looking at the stator suction side in Fig. 10a, where the negative derivative on the whole surface means that a reduction of the stator total pressure loss would be obtained by displacing the stator blade suction side outwards, but that

would create a detrimental impact on the stage total pressure ratio, since this metric has an opposite sensitivity on the fore portion of the blade, as seen in Fig. 10c.

The danger of performing single blade row optimization not only occurs for the stator, as described before, but also for the rotor, although not as severe for the present case. Referring to the rotor suction side in Fig. 9b, there is a small region of negative derivative of the rotor total pressure ratio at the trailing edge near the blade tip. The same region is also present when considering the stage total pressure ratio in Fig. 9c, although not as extended. Therefore, there could

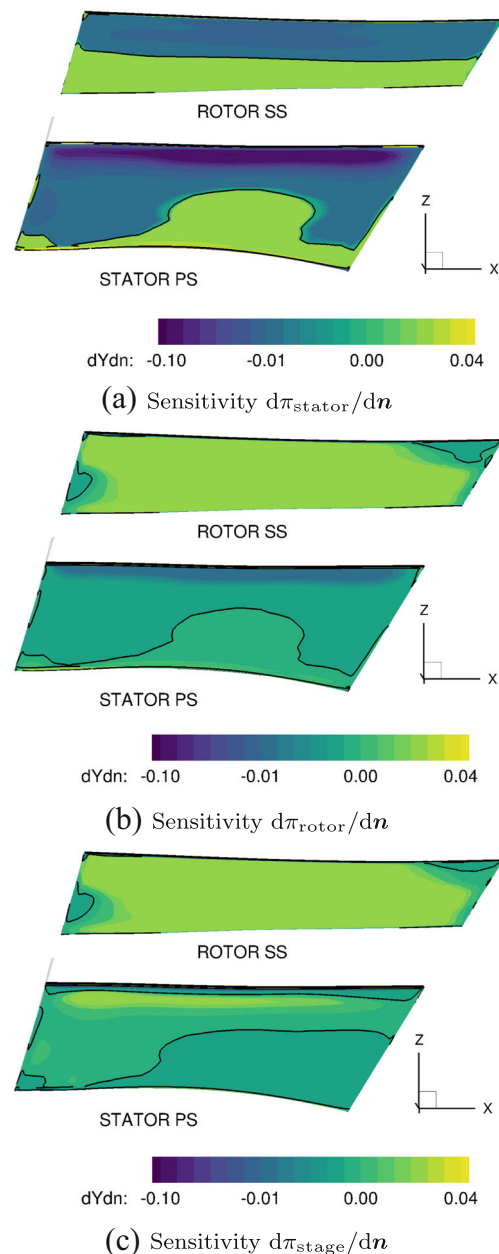


Fig. 9 Sensitivity of pressure ratio metrics to blade shape in normal direction—stator pressure side and rotor suction side view

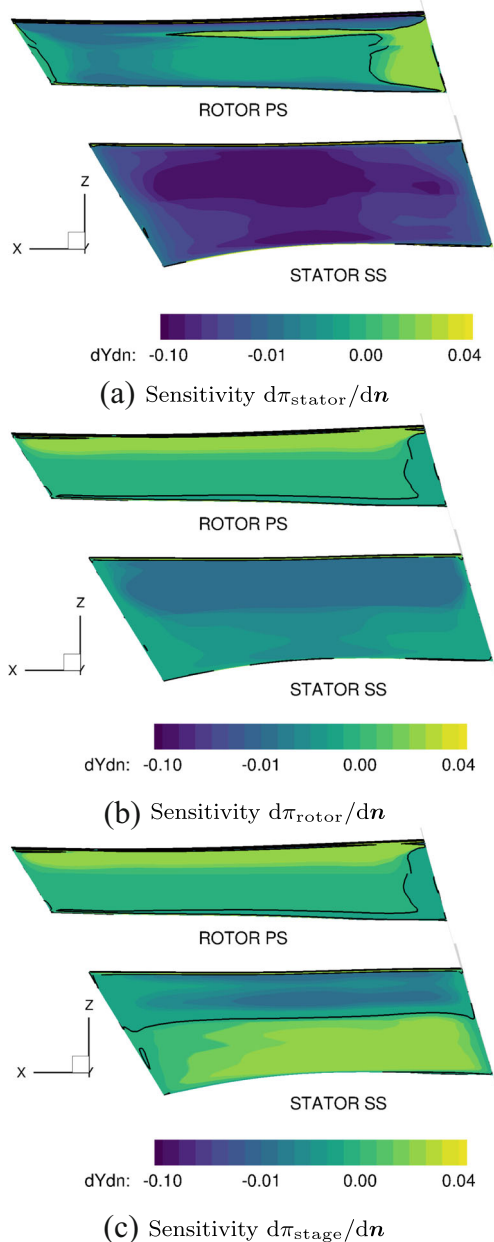


Fig. 10 Sensitivity of pressure ratio metrics to blade shape in normal direction—stator suction side and rotor pressure side view

potentially occur a detrimental effect on the overall stage if the rotor blade is changed in this mismatched region having in mind just to improve the rotor total pressure ratio.

This clearly demonstrates the danger of optimizing individual rows or, in other words, the benefit that considering the coupled stator-rotor system would bring to the overall design. Were it not for the coupled stator-rotor performance sensitivity computed, thanks to the developed turbomachinery multi-row adjoint solver, these behaviors would not been possible to capture, possibly leading the designer to perform erroneous design changes.

6 Performance sensitivity to endwall shape

As mentioned in Section 1, secondary flows that occur in the endwall regions of turbomachine components have a significant impact on their performance. As such, the sensitivity information given by the adjoint solver regarding the endwall shape can provide very insightful information to a designer on how to mitigate the adverse effect of these flows on the performance by tuning the hub and/or casing geometries.

In this section, the adjoint-based sensitivities presented are projected onto the radial direction, through the transformation

$$\frac{d\mathcal{I}}{dr} = \frac{d\mathcal{I}}{dx} \frac{dx}{dr} + \frac{d\mathcal{I}}{dy} \frac{dy}{dr} = \frac{d\mathcal{I}}{dx} \cos(\theta) + \frac{d\mathcal{I}}{dy} \sin(\theta), \quad (18)$$

where θ is the tangential angle in cylindrical coordinates measured from the x - to the y -axis.

The sensitivity of the stator loss coefficient, and the rotor and stage efficiencies to the radial position of the mesh grid nodes of the hub is presented in Fig. 11, while the sensitivity of the stator total pressure loss, rotor total pressure ratio, and stage total pressure ratio is shown in Fig. 12. The sensitivity to radial position is obtained from the sensitivity to x - and y -coordinates with the transformation defined by (18), meaning that, for the presented figures, positive values of $d\eta/dr_{\text{hub}}$ indicate that moving the surface nodes in the direction of the casing (or the viewer) would increase the efficiency. It should also be noted that the computational domains are repeated axially in these figures to better visualize the sensitivity results.

The sensitivity of the efficiency metrics (Fig. 11) is higher than that of the pressure ratio metrics (Fig. 12) relative to endwall contouring, similarly to what was also observed relative to the blade shape in Section 5.

Observing Figs. 11c and 12c, the sensitivities of the stage efficiency and pressure ratio reveal that there is a significant hub region close to the stator pressure side where the derivatives present a positive value. This means that a change in the hub radius, in this stator region, aiming to increase stage efficiency (desired) would also increase the stage total pressure ratio (undesired). The rotor hub also presents conflicting impact on these two performance metrics, particularly in the region at about 50% of the chord and roughly equidistant between the rotor blades. Thus, similarly to the blade shape analyses made in Section 5, contouring the hub shape can also lead to conflicting results.

Focusing on the efficiency metrics, Fig. 11a contains the stator pressure loss coefficient sensitivity to stator hub shape, that would be used in the single stator optimization aimed at reducing its loss. Comparing it to sensitivity of the stage efficiency to the stator hub in Fig. 11c, whose

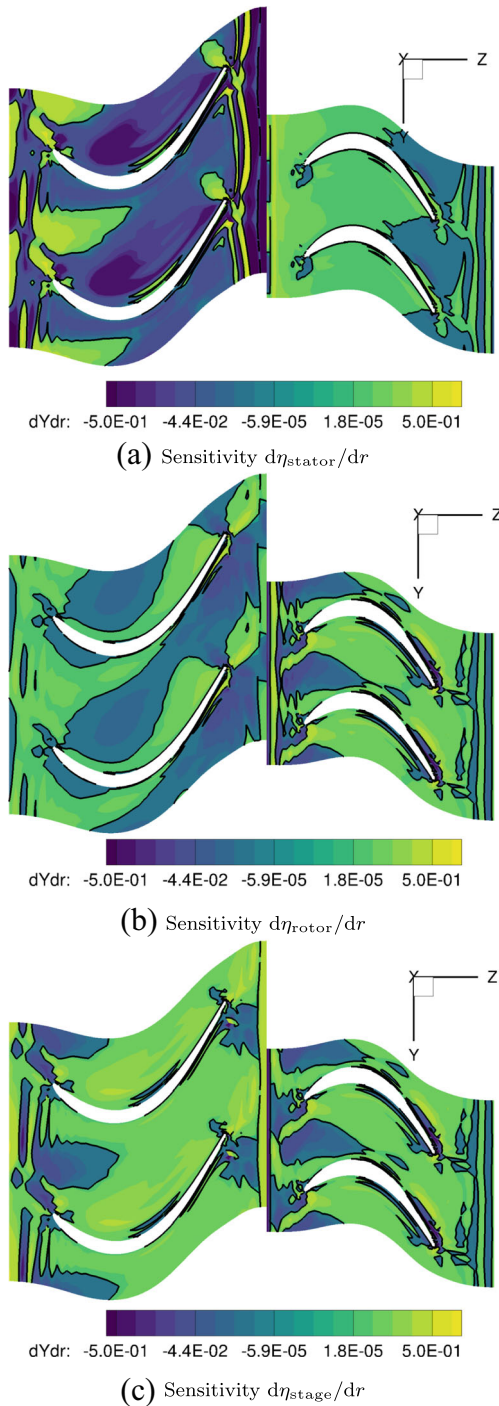


Fig. 11 Sensitivity of efficiency metrics to radial perturbation of hub grid nodes $d\eta/dr_{\text{hub}}$ (normalized)

derivatives are opposite in sign, it shows that the reduction of the stator loss coefficient by means of endwall contouring of the stator hub would lead to an overall increase of the stage efficiency.

The same findings apply when considering the optimization of the isolated rotor or the whole stage, since the

sensitivity of the rotor efficiency (in Fig. 11b) and the sensitivity of the stage efficiency (in Fig. 11c) to the hub rotor shape are very similar.

The observations made regarding the effect of single stator or single rotor efficiency optimization on the overall stage efficiency can also be made relative to the other

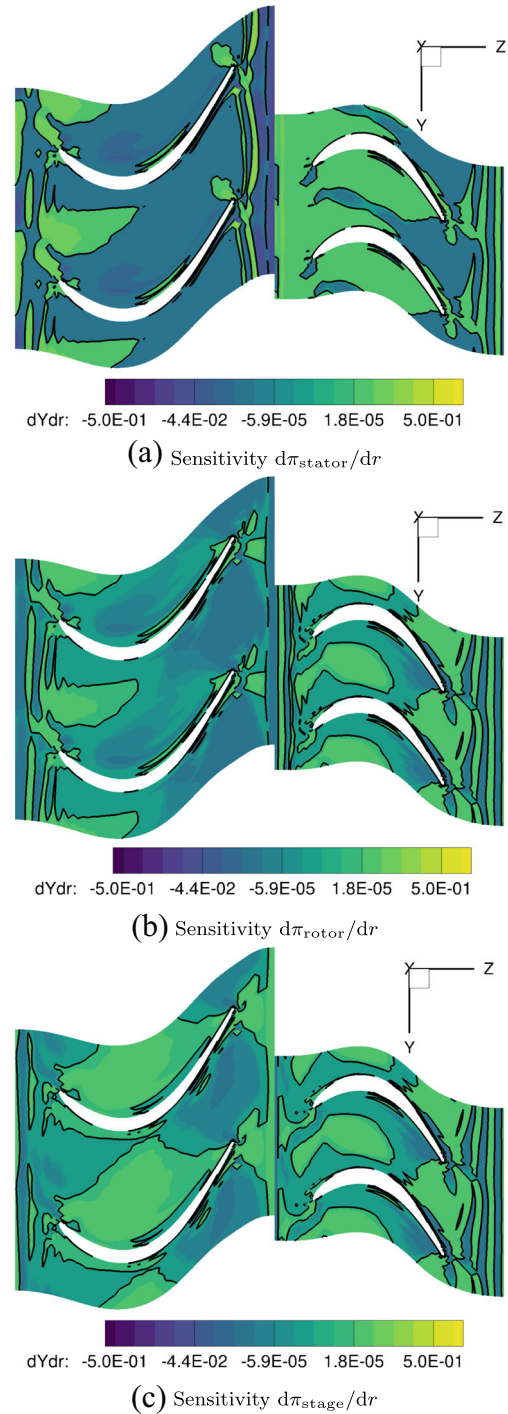


Fig. 12 Sensitivity of pressure ratio metrics to radial perturbation of hub grid nodes $d\pi/dr_{\text{hub}}$ (normalized)

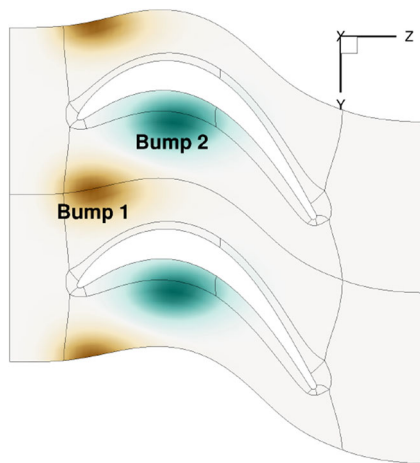


Fig. 13 Hicks-Henne bumps imposed on the rotor hub

metrics of pressure ratio. Looking at the sensitivity of the stator total pressure loss in Fig. 12a and comparing it with the sensitivity of the stage total pressure ratio in Fig. 12c, focusing on the stator hub shape, there is a large conflicting region (different derivative signs) up to about 90% streamwise (from leading edge to almost trailing edge). This once again means that contouring the stator hub for reducing the stator total pressure loss (desired) leads to an unexpected increase of the stage total pressure ratio (undesired).

7 Improving stage efficiency with endwall contouring

Based on the findings in Section 6, we present in this section an attempt to improve the stage efficiency by contouring the hub of the rotor thru the application of two bumps on

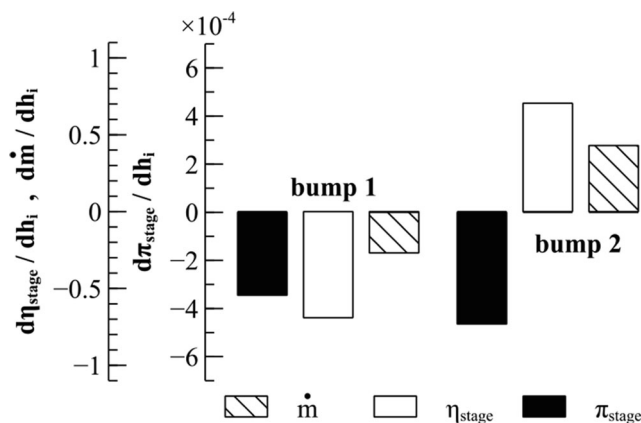


Fig. 14 Sensitivity of stage performance metrics to bumps height

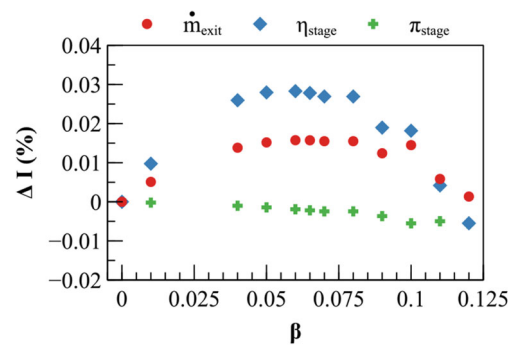


Fig. 15 Variation of the stage performance metrics with the perturbation step parameter β

its surface. We selected the locations of the bumps from the analysis of the adjoint-based sensitivities to the hub geometry presented in Fig. 11c, and selected their height using a manual line search procedure.

7.1 Hicks-Henne bumps

Looking again at Fig. 11c, it shows that the hub region between the blades, at a streamwise location equal to the leading edge of the rotor blade, presents high (negative) influence on the stage efficiency. The hub region close to the pressure side of the rotor blade also presents relatively high (positive) influence. As such, we selected these two regions to impose the bumps, which are represented in Fig. 13.

The bumps are imposed on the hub by perturbing its surface in the radial direction by an amount given by

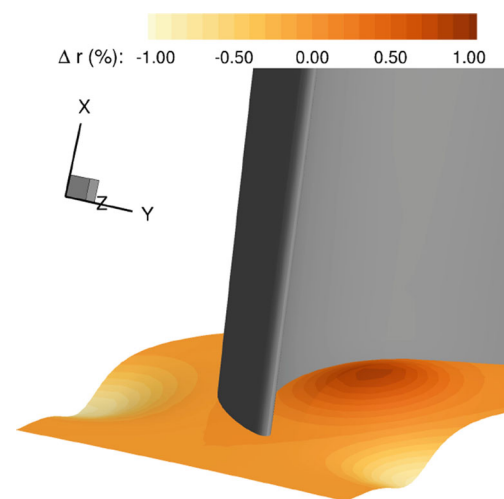
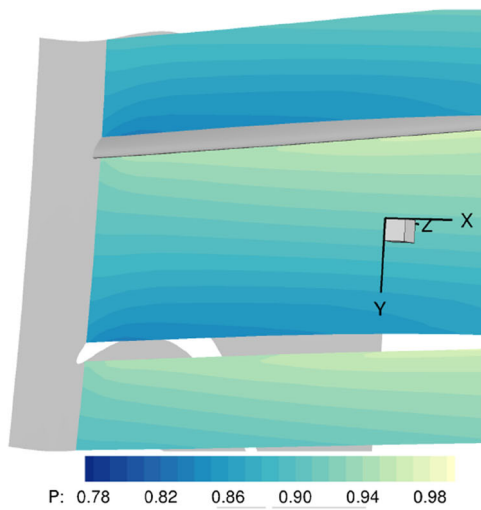
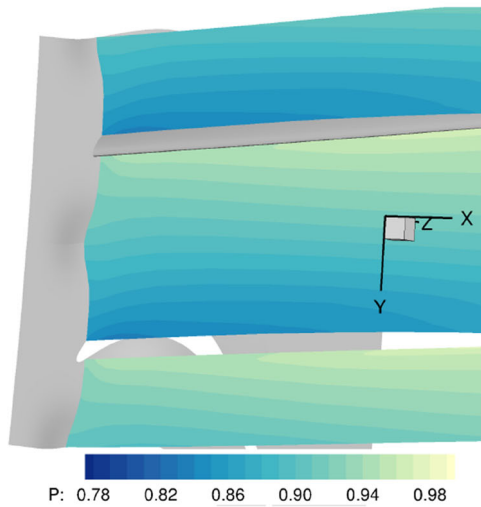


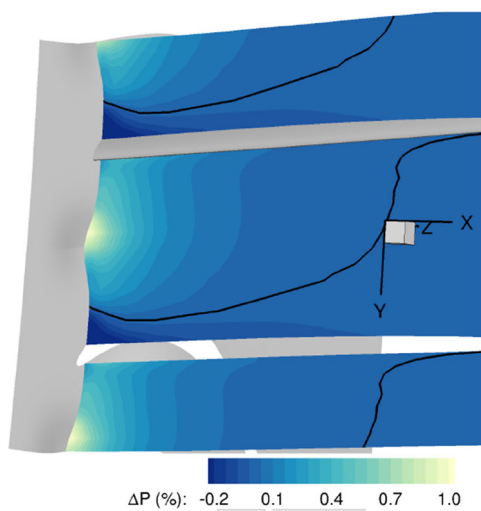
Fig. 16 Radial displacement imposed on the rotor hub (in % of blade span)



(a) Original pressure field

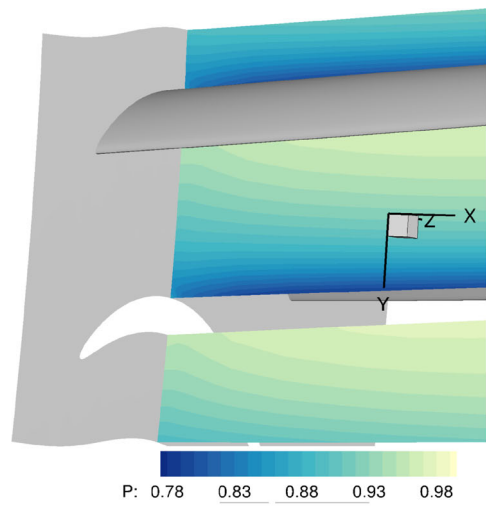


(b) Modified pressure field

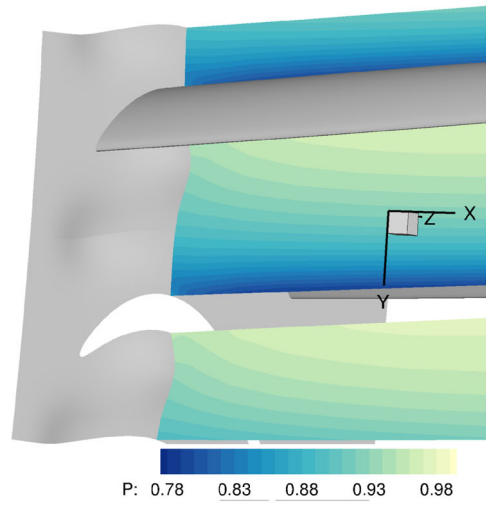


(c) Relative pressure difference

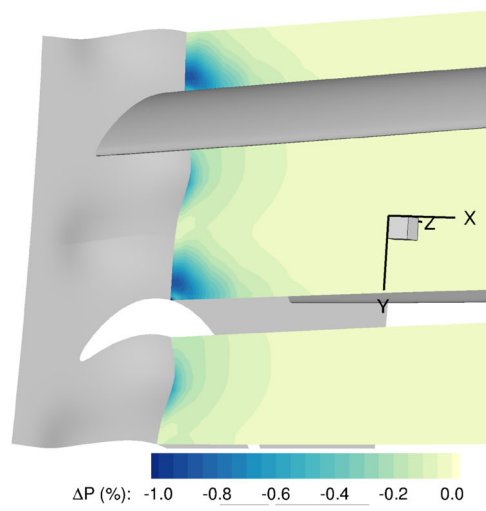
Fig. 17 Pressure field change due to the two bumps on the rotor hub at an XY plane centered at bump 1



(a) Original pressure field



(b) Modified pressure field



(c) Relative pressure difference

Fig. 18 Pressure field change due to the two bumps on the rotor hub at an XY plane centered at bump 2

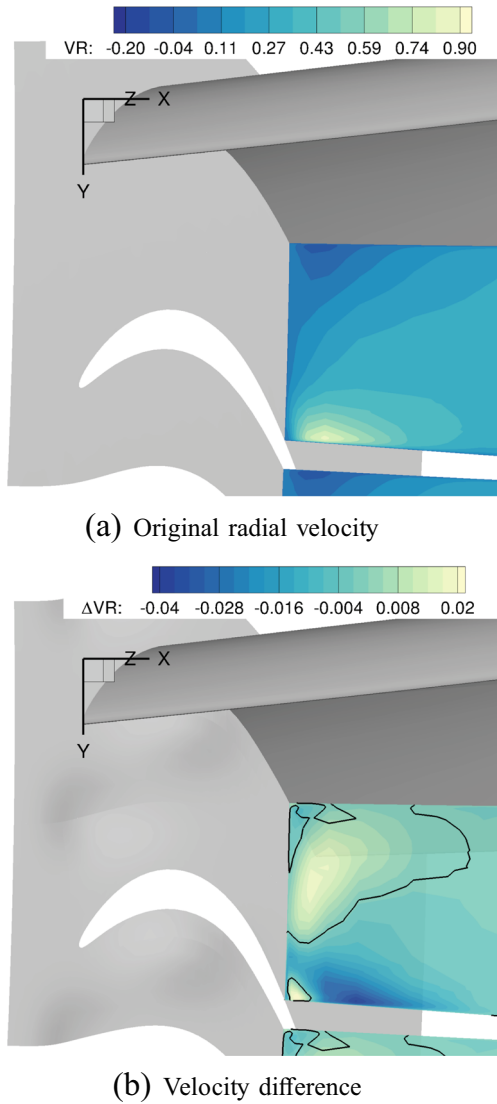


Fig. 19 Radial velocity change due to the two bumps in the rotor hub at an XY plane at 85% chord (normalized values)

the Hicks-Henne bump function (Hicks and Henne 1978), defined as

$$\Delta X_{s,i} = \sum_{j=1}^{N_b} h_j \left[\sin \left(\pi \hat{x}_{1,i}^{\frac{\log 0.5}{\log t_{c,1,j}}} \right) \right]^{t_{w,1,j}} \times \left[\sin \left(\pi \hat{x}_{2,i}^{\frac{\log 0.5}{\log t_{c,2,j}}} \right) \right]^{t_{w,2,j}}, \quad (19)$$

where N_b is the number of bumps; h_j is the amplitude (peak height) of bump j ; $\hat{x}_{1,j}$ and $\hat{x}_{2,j}$ are the normalized coordinates of vertex i in the two directions θ and z , respectively; $t_{c,1,j}$ and $t_{c,2,j}$ define the location of the peak of bump j ; and $t_{w,1,j}$ and $t_{w,2,j}$ define how spread the bump is in each location (higher values lead to a less spread bump).

As mentioned in Section 2.3, the sensitivity to the Hicks-Henne bump parameters is obtained from a first-order finite difference approximation, computed using the original and modified grids. The interior grid nodes are modified using an inverse distance weight interpolation scheme (Shepard 1968) as

$$\Delta X_{v,j} = \frac{\sum_{i=1}^{N_s} \Delta X_{s,i} / r_{j,i}^p}{\sum_{i=1}^{N_s} 1 / r_{j,i}^p}, \quad (20)$$

where N_s is the number of surface nodes, $r_{j,i}$ is the distance from the interior node j to the surface node i , and p is the power parameter.

7.2 Line search procedure

We started by computing the adjoint-based sensitivities of the various performance metrics using (8), where the mesh perturbation sensitivity $dX/d\alpha$ was computed using forward finite differences from the unperturbed and perturbed meshes. The resultant gradients are presented in Fig. 14.

These gradients indicate that (i) introducing a negative bump (inwards) near the leading edge (bump 1) would translate into an increase of the stage efficiency, total pressure ratio, and mass flow; (ii) a positive displacement (outwards) of bump 2 would translate into an increase of the stage efficiency and mass flow while reducing the stage total pressure ratio.

Should this information be used by a gradient-based numerical optimization algorithm, such as steepest descent, the bump height parameters, h_1 and h_2 , would be perturbed along the search direction according to

$$\mathbf{h} = (h_1, h_2) = \beta \left(\frac{d\eta_{\text{stage}}}{dh_1}, \frac{d\eta_{\text{stage}}}{dh_2} \right), \quad (21)$$

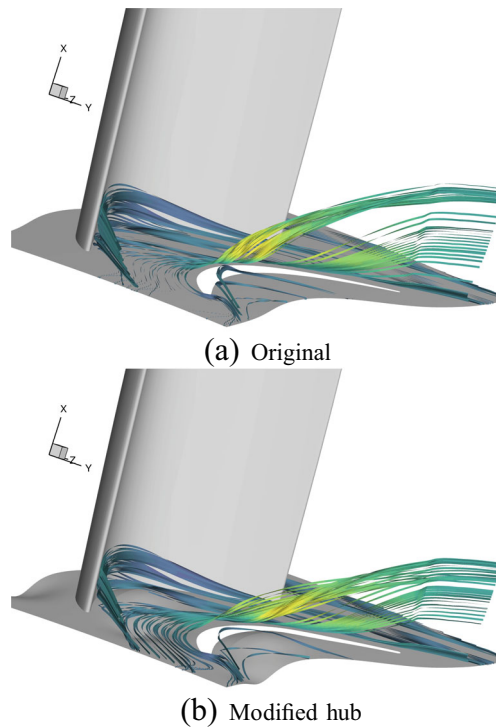
where a line search procedure would be performed to find the optimal value of β that maximizes η_{stage} .

In this work, we performed manually a line search, similarly to what an optimizer would do, resulting in the values presented in Fig. 15, where the variation of \dot{m}^{exit} , η_{stage} and π_{stage} relative to the baseline is plotted for different values of β .

The behavior of the stage efficiency is as one would expect, increasing with β up to a certain point (between 0.05 and 0.08 in the present case) and then decreasing. The mass flow at the exit of the stage presents a similar variation (in percentage) to the stage efficiency, although with smaller magnitude. On the other hand, the stage total pressure ratio shows a slight decrease as the bumps are perturbed following the search direction given by $d\eta_{\text{stage}}/d\mathbf{h}$.

We selected a value of $\beta = 0.06$ from Fig. 15, which is roughly near the value that maximizes η_{stage} , that translates into an efficiency improvement of approximately 0.03%.

Fig. 20 Streamtraces along the rotor blade passage



The relatively small expected efficiency improvement can be explained by the already tuned low-pressure turbine stage test case we used, and also it might indicate that the number of bumps should be extended to provide a larger design space.

The two bumps present a maximum height of approximately 0.8% of the rotor blade span, as shown in Fig. 16.

7.3 Improved flow

The improvement of the stage efficiency with the application of the “optimal” bumps, found in the previous section, is the result of a modified flow field. Here, we try to identify the main flow features responsible for the stage efficiency improvement.

Figure 17 presents the original and modified pressure fields (normalized values) due to the presence of the two bumps, in an XY plane located at the center of the first bump, as well as the relative difference between the two, computed as

$$\Delta p = \frac{(p)_{\text{bumps}} - (p)_{\text{base}}}{(p)_{\text{base}}} \times 100, \quad (22)$$

meaning that positive difference values represent an increase from the baseline to the modified pressure flow field. The increase of pressure due to the negative bump

(concave) is evident but there is also a reduction in pressure near the suction side of the blade.

Figure 18 presents the pressure field in an XY plane located at the center of the second bump. In this case, the presence of the bumps only reduces the pressure in that plane, particularly in the region near suction side of the blade.

Figure 19 shows the original radial velocity component as well as its variation due to the presence of the two bumps, in an XY plane located at 85% of the blade chord. Both the velocity and difference values are normalized by the maximum radial velocity in the rotor passage.

The two bumps create a deficit in the velocity in the radial direction (Fig. 19b), reducing the mixture of the boundary layer with the flow. This region contains relatively high velocity in the radial direction, as also seen in Fig. 20a that illustrates a set of streamtraces along the rotor blade passage.

The secondary flow created at the interface hub blade is clearly visible in the streamtraces. The effect of the bumps is visible in Fig. 20b, where the streamtraces remain closer to the surface than in the original geometry, reducing its detrimental impact on the performance, thus increasing the efficiency.

The original radial velocity field in a XY plane located behind the rotor blade is presented in Fig. 21a, normalized by the maximum radial velocity in the rotor passage. The

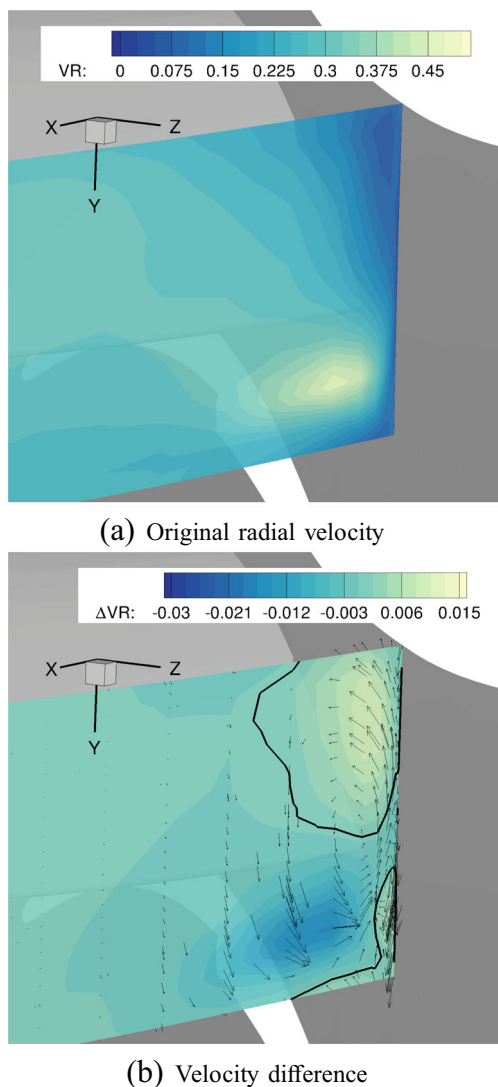


Fig. 21 Radial velocity change due to the two bumps in the rotor hub at an XY plane behind blade (normalized values)

region of higher mixture of the boundary layer, highlighted in Fig. 20, is visible from the higher values of radial velocity below the trailing edge.

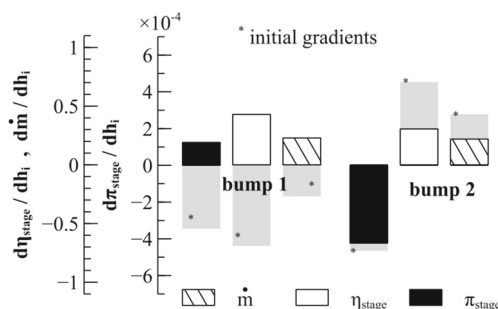


Fig. 22 Sensitivity of stage performance metrics to bumps height in modified geometry

The presence of the two bumps mitigate this by trying to homogenize the radial velocity profile in the pitchwise direction, which is clear in Fig. 21b, where the variation in the radial velocity due to the bumps is presented, along with the vector field of the variation of velocity.

Figure 22 presents the adjoint-based gradients of the performance metrics presented in Fig. 14 considering the modified geometry, obtained by computing the adjoint solution from the new modified flow solution and following the procedure previously mentioned.

While there is a clear reduction in the magnitude of the gradients, this is unsurprisingly evident for the case of stage efficiency, that was used as objective function to be maximized in the steepest descent iteration performed. It also shows that further iterations would be required to converge the unconstrained optimization since the stage efficiency gradient is still non-zero.

8 Conclusions

We made use of an adjoint solver for turbomachinery sensitivity analysis, capable of handling multi-row problems, to study a low-pressure turbine stator-rotor stage. We studied the influence of blades and hub shapes on a set of relevant performance metrics, where we presented the differences between the sensitivities of single component (individual stator and individual rotor) metrics and the whole stage (coupled stator-rotor). We have found contradictory sensitivities, not only between themselves but also between single or coupled components. While the former can be dealt with trade-off studies or constrained optimization, the latter can pose a challenger to the designer since individual component optimization can actually lead to an undesired coupled performance loss. This highlights the importance of coupling the various rows of turbomachinery components not only in their analysis but mainly in their design.

As a demonstration of the use of the adjoint-based stage coupled sensitivities, we imposed two bumps on the rotor hub surface, representing a simple case of endwall contouring, where we achieved an improvement of the stage efficiency. We were then able to correlate the changes in the flow field that resulted from the endwall contouring with the achieved performance gain, particularly in terms of secondary flows.

9 Replication of results

The results of this paper can be reproduced using any solver capable of solving the RANS governing equations and respective adjoint equations. All the numerical methods

used are referenced throughout the paper. The computer code used to obtain the results presented in this paper as well as the blade geometry are proprietary and, as such, cannot be provided.

Acknowledgments The authors are thankful to General Electric for giving permission to publish this paper.

Funding information This work was supported by the Fundação para a Ciência e Tecnologia (FCT), Portugal, through the scholarship SFRH/BD/97521/2013; and through Institute of Mechanical Engineering (IDMEC), under the Associated Laboratory for Energy, Transports and Aeronautics (LAETA) project UID/EMS/50022/2019.

Compliance with ethical standards

Conflict of interest The authors declare that they have no conflict of interest.

References

- Agarwal D, Robinson TT, Armstrong CG, Kapellos C (2018) Enhancing CAD-based shape optimisation by automatically updating the CAD model's parameterisation. *Structural and Multidisciplinary Optimization*. <https://doi.org/10.1007/s00158-018-2152-7>
- Backhaus J, Schmitz A, Frey C, Sagebaum M, Mann S, Nagel M, Gauger NR (2017) Application of an algorithmically differentiated turbomachinery flow solver to the optimization of a fan stage. *American Institute of Aeronautics and Astronautics*. <https://doi.org/10.2514/6.2017-3997>
- Balay S, Abhyankar S, Adams M, Brown J, Brune P, Buschelman K, Eijkhout V, Gropp W, Kaushik D, Knepley M et al (2014) PETSc Users Manual Revision 3.5
- Benamara T, Breikopf P, Lepot I, Sainvitu C, Villon P (2017) Multi-fidelity POD surrogate-assisted optimization: concept and aero-design study. *Struct Multidiscip Optim* 56(6):1387–1412. <https://doi.org/10.1007/s00158-017-1730-4>
- Beselt C, Eck M, Peitsch D (2014) Three-dimensional flow field in highly loaded compressor cascade. *J. Turbomach.* 136(10):101007. <https://doi.org/10.1115/1.4028083>
- Chirkov DV, Ankudinova AS, Kryukov AE, Cherny SG, Skorospelov VA (2018) Multi-objective shape optimization of a hydraulic turbine runner using efficiency, strength and weight criteria. *Struct Multidiscip Optim* 58(2):627–640. <https://doi.org/10.1007/s00158-018-1914-6>
- Corral R, Gisbert F (2008) Profiled end wall design using an adjoint Navier-Solver. *J. Turbomach.* 130(2):021011. <https://doi.org/10.1115/1.2751143>
- Ding L, Lu Z, Guo T (2014) An efficient dynamic mesh generation method for complex multi-block structured grid. *Adv. Appl. Math. Mech.* 6(01):120–134. <https://doi.org/10.4208/aamm.2013.m199>
- Duan Y, Fan Z, Wu W, Chen T (2018) Study on global aerodynamic shape optimization of transonic compressor blade. *International Journal of Turbo & Jet-Engines* 0(0). <https://doi.org/10.1515/tjj-2018-0013>
- Giles MB, Pierce NA (2000) An introduction to the adjoint approach to design. *Flow Turbul. Combust.* 65(3-4):393–415
- Hicks RM, Henne PA (1978) Wing design by numerical optimization. *J Aircr* 15(7):407–412. <https://doi.org/10.2514/3.58379>
- Holmes DG (2008) Mixing planes revisited: a steady mixing plane approach designed to combine high levels of conservation and robustness. In: *Proceedings of ASME Turbo Expo 2008: power for land, sea and air*, Berlin, Germany, pp 2649–2658. <https://doi.org/10.1115/GT2008-51296>
- Jameson A (1988) Aerodynamic design via control theory. *J Sci Comput* 3(3):233–260
- Jameson A, Martinelli L, Pierce NA (1998) Optimum aerodynamic design using the Navier-Stokes equations. *Theor Comput Fluid Dyn* 10(1-4):213–237
- Jameson A, Shankaran S, Martinelli L, Haimes B (2004) Aerodynamic shape optimization of complete aircraft configurations using unstructured grids. In: *42nd AIAA aerospace sciences meeting and exhibit*, American institute of aeronautics and astronautics, Reno, Nevada. <https://doi.org/10.2514/6.2004-533>
- Joly MM, Verstraete T, Paniagua G (2014) Multidisciplinary design optimization of a compact highly loaded fan. *Struct Multidiscip Optim* 49(3):471–483. <https://doi.org/10.1007/s00158-013-0987-5>
- Lamouin HJ, Waggenspack NN (1994) NURBS-based free-form deformations. *IEEE Comput. Graph. Appl.* 14(6):59–65. <https://doi.org/10.1109/38.329096>
- Launder BE, Spalding DB (1972) *Mathematical models of turbulence*. Academic Press, London
- Luke E, Collins E, Blades E (2012) A fast mesh deformation method using explicit interpolation. *J Comput Phys* 231(2):586–601. <https://doi.org/10.1016/j.jcp.2011.09.021>
- Luo J, Liu F, McBean I (2015) Turbine blade row optimization through endwall contouring by an adjoint method. *J Propuls Power* 31(2):505–518. <https://doi.org/10.2514/1.B35152>
- Marta AC, Shankaran S (2013) On the handling of turbulence equations in RANS adjoint solvers. *Comput. Fluids* 74:102–113. <https://doi.org/10.1016/j.compfluid.2013.01.012>
- Marta AC, Shankaran S (2014) Assessing turbomachinery performance sensitivity to boundary conditions using control theory. *J Propuls Power* 30(5):1–14. <https://doi.org/10.2514/1.B35087>
- Marta AC, Shankaran S, Wang Q, Venugopal P (2013) Interpretation of adjoint solutions for turbomachinery flows. *AIAA J* 51(7):1733–1744. <https://doi.org/10.2514/1.J052177>
- Min J, Harris D, Ting J (2011) Advances in ceramic matrix composite blade damping characteristics for aerospace turbomachinery applications. In: *52nd AIAA/ASME/ASCE/AHS/ASC structures, structural dynamics and materials conference* American institute of aeronautics and astronautics, Denver, Colorado. <https://doi.org/10.2514/6.2011-1784>
- Mueller L, Verstraete T (2017) CAD integrated multipoint adjoint-based optimization of a turbocharger radial turbine. *International Journal of Turbomachinery, Propulsion and Power* 2(3):14. <https://doi.org/10.3390/ijtpp2030014>
- Mykhaskiv O, Banović M, Auriemma S, Mohanamuraly P, Walther A, Legrand H, Müller JD (2018) NURBS-based and parametric-based shape optimization with differentiated CAD kernel. *Comput-Aided Des Appl* 15(6):916–926. <https://doi.org/10.1080/16864360.2018.1462881>
- Pierret S, Filomeno Coelho R, Kato H (2007) Multidisciplinary and multiple operating points shape optimization of three-dimensional compressor blades. *Struct Multidiscip Optim* 33(1):61–70. <https://doi.org/10.1007/s00158-006-0033-y>
- Pironneau O (1974) On optimum design in fluid mechanics. *J Fluid Mech* 64(01):97–110. <https://doi.org/10.1017/S0022112074002023>
- Poehler T, Niewoehner J, Jeschke P, Guendogdu Y (2015) Investigation of Nonaxisymmetric endwall contouring and three-dimensional airfoil design in a 1.5-stage axial turbine—part I: Design and novel numerical analysis method. *J Turbomach* 137(8):081009. <https://doi.org/10.1115/1.4029476>
- Reutter O, Rozanski M, Hergt A, Nicke E (2017) Advanced endwall contouring for loss reduction and outflow homogenization for an optimized compressor cascade. *International*

- journal of turbomachinery, Propulsion and Power 2(1):1. <https://doi.org/10.3390/ijtpp2010001>
- Rodrigues SS, Marta AC (2018) Adjoint formulation of a steady multistage turbomachinery interface using automatic differentiation. *Computers & Fluids*. <https://doi.org/10.1016/j.compfluid.2018.09.015>
- Sauer H, Müller R, Vogeler K (2001) Reduction of secondary flow losses in turbine cascades by leading edge modifications at the endwall. *J Turbomach* 123(2):207. <https://doi.org/10.1115/1.1354142>
- Schneider CM, Schrack D, Kuerner M, Rose MG, Staudacher S, Guendogdu Y, Freygang U (2013) On the unsteady formation of secondary flow inside a rotating turbine blade passage. *J Turbomach* 136(6):061004. <https://doi.org/10.1115/1.4025582>
- Shepard D (1968) A two-dimensional interpolation function for irregularly-spaced data. In: Proceedings of the 1968 23rd ACM national conference on - ACM Press, Not known, pp 517–524, <https://doi.org/10.1145/800186.810616>
- Walther B, Nadarajah S (2015) Optimum shape design for multirow turbomachinery configurations using a discrete adjoint approach and an efficient radial basis function deformation scheme for complex multiblock grids. *J Turbomach* 137(8):081006–081006. <https://doi.org/10.1115/1.4029550>
- Wilcox DC (2008) Formulation of the k- ω Turbulence Model Revisited. *AIAA J* 46(11):2823–2838. <https://doi.org/10.2514/1.36541>
- Yu K, Yang X, Yue Z (2011) Aerodynamic and heat transfer design optimization of internally cooling turbine blade based different surrogate models. *Struct Multidiscip Optim* 44(1):75–83. <https://doi.org/10.1007/s00158-010-0583-x>

Publisher's note Springer Nature remains neutral with regard to jurisdictional claims in published maps and institutional affiliations.